

**GEORGE MISSION - STRUCTURES SUBTEAM**  
**CONCEPT OF OPERATIONS**  
**FALL 2023**



**Massachusetts Institute of Technology**  
**Department of Aeronautics and Astronautics**

Course 16.83: Space Systems Engineering

Instructor: Professor Kerri Cahoy

**Structures Team Members**

Pablo Arroyo Yatin Chandar Hillel Dei

December 03, 2023

# Table of Contents

List of Figures . . . . .	iii
List of Tables . . . . .	iii
List of Abbreviations . . . . .	iv
<b>1 Introduction &amp; Overview - H. Dei</b>	<b>1</b>
1.1 Deliverables . . . . .	2
<b>2 Point-of-Departure Design - P. Arroyo, H. Dei</b>	<b>2</b>
<b>3 Mass Properties - H. Dei</b>	<b>3</b>
3.1 Coordinate Frames . . . . .	3
3.2 Mass Table & Margins of Safety . . . . .	3
<b>4 Materials Selection Trade - Y. Chandar</b>	<b>5</b>
4.1 Yield Strength/Density Ratio . . . . .	5
4.2 Cost and Density . . . . .	5
4.3 Environment Characteristics . . . . .	5
4.4 Manufacturing Considerations . . . . .	6
4.5 Flight Heritage . . . . .	6
4.6 Selection . . . . .	6
<b>5 Structural Analysis - H. Dei, P. Arroyo, Y. Chandar</b>	<b>6</b>
5.1 Loading Analysis Under Launch Conditions & Dynamic Analysis . . . . .	6
5.2 Thermal Stress and Loading Analysis for Heat Redistribution System . . . . .	9
<b>6 Conclusion - H. Dei</b>	<b>10</b>
<b>References</b>	<b>11</b>
<b>Appendices</b>	<b>12</b>
<b>A L1 Requirements</b>	<b>12</b>
<b>B Power System Structure Trade - P. Arroyo, Y. Chandar</b>	<b>14</b>
B.1 Solar Arrays . . . . .	14
B.2 RTGs . . . . .	14
B.3 Recommendations . . . . .	14
<b>C Vibrational Analysis</b>	<b>15</b>
<b>D Loading Analysis for Deployable Mechanisms</b>	<b>16</b>

## List of Figures

Figure 1	Cassini Threeview - created by Pablo Arroyo.	2
Figure 2	Credit: Europa Clipper Coordinates in Orbit, courtesy of Kivelson et al [3].	3
Figure 3	Subsystem Position and Movement, as point masses - created by Hillel Dei.	4
Figure 4	Falcon Heavy Payload Fairing Dimensions, credit to SpaceX [4].	7
Figure 5	Falcon Heavy PSD Curve, credit to SpaceX [4].	8
Figure 6	Rough CAD model (without boom) normal mode frequencies created by Pablo Arroyo	9
Figure 7	Illustration of stress on fluid lines during thermal cycling, from of Burdick et al [6].	9
Figure 8	Inertial welding at material junctions, credit to Burdick et al [6].	10
Figure 9	Joint stresses, credit to Burdick et al [6].	10
Figure 10	Rough CAD model vibration response, without boom deployed; created by Pablo Arroyo	15
Figure 11	Rough CAD model vibration response, with boom deployed; created by Pablo Arroyo	15
Figure 12	Rough CAD model vibration response table, with boom deployed; created by Pablo Arroyo	16
Figure 13	Kinematics of solar array deployment, credit to M. Arya [5].	16
Figure 14	Force Diagram of solar array deployment, credit to M. Arya [5].	17

## List of Tables

Table 1	Mass Budget.	4
---------	--------------	---

## **List of Abbreviations**

**GEORGE** Going to Europa for the Orbital Recovery of Geyser Emissions

**ADCS** Attitude Determination and Control System

**RTG** Radioisotope thermoelectric Generator

**PSD** Power Spectral Density

**CFRP** Carbon Fiber Reinforced Polymer

**CTE** Coefficient of Thermal Expansion

# 1 Introduction & Overview - H. Dei

To summarise the design goals of the GEORGE mission, we aim to:

1. Investigate the nature and patterns of Europan cryovolcanism.
2. Identify of the causes of this geographic activity.
3. Analyze of the frequency of any occurrences.
4. Evaluate the geographical distribution of this activity.

According to our mission goals, there is a clear need to detect events, so we, the Structures subteam, are responsible for ensuring the system is capable of providing this functionality, upon arrival at the mission location, and for as long as possible beyond then, through the design and analysis of a chassis to fulfill these requirements. As a sub-team our fundamental goals are to facilitate:

1. General chassis design and instrument integration, including:
  - (a) Instrument mounting geometry
  - (b) Resonance mode avoidance
  - (c) Integration feasibility
2. Mass tracking
3. Coordinate selection

GEORGE's objectives, as proposed by the Science and Systems subteams, align closely with several previous missions, notably including the Cassini, Europa Clipper, and Juno probes and the upcoming Juice probes. Drawing inspiration from their design strategies, we've made some key modifications to meet our unique requirements. One significant change is our preference for nuclear power over the more traditional solar power. This decision stems from the specific challenges posed by our orbital trajectory. While solar power is a proven solution, the demanding science goals of GEORGE, coupled with the need for enhanced maneuverability and the advantage of reduced mass, make nuclear power an invaluable asset. In this section, we aim to shed light on the various forces impacting GEORGE's structure, delve into the system's layout and mechanical implications, and discuss crucial aspects of GEORGE's static and dynamic loading conditions, especially during launch.

Our system's design is heavily dependent on the choices made by other teams regarding hardware selection, around which we have to conceptualize our design. An essential part of our analysis involves examining how sensitive parameters like the center of mass and the inertial matrix respond to variations in the geometry and positioning of other subsystems. We include comprehensive calculations for the expected load during launch, as well as vibrational analysis. The CAD models are crafted with sufficient detail to accurately depict mass properties, but they remain adaptable to accommodate the expected frequent changes in the spacecraft's component masses and positions.

## 1.1 Deliverables

1. CAD models and threeview drawing of point-of-departure GEORGE chassis iteration and its components.
2. Normal Mode Vibrational Analysis of GEORGE for the first 12 modes.
3. Finite Element Analysis of GEORGE to determine exact vibrational loading at potentially problematic locations in a given launch environment.
4. Mass Properties:
  - (a) Spreadsheet of Center of Mass of each subsystem and mass budgets.
  - (b) Inertia Matrix.
5. Margins of Safety and appropriate justifications.
6. Structural analysis of all subsystems in isolation and fully interfaced.
7. Ashby chart with Selection Index to justify choice in thermal protection material.
8. A point-of-departure design that meets the requirements of both the Thermal and Science Subteams.

## 2 Point-of-Departure Design - P. Arroyo, H. Dei

Given the use of RTGs, the current working CAD model is a rough approximation of the Cassini spacecraft. This model is a placeholder and will be further refined as the other subsystems finalize components and requirements.

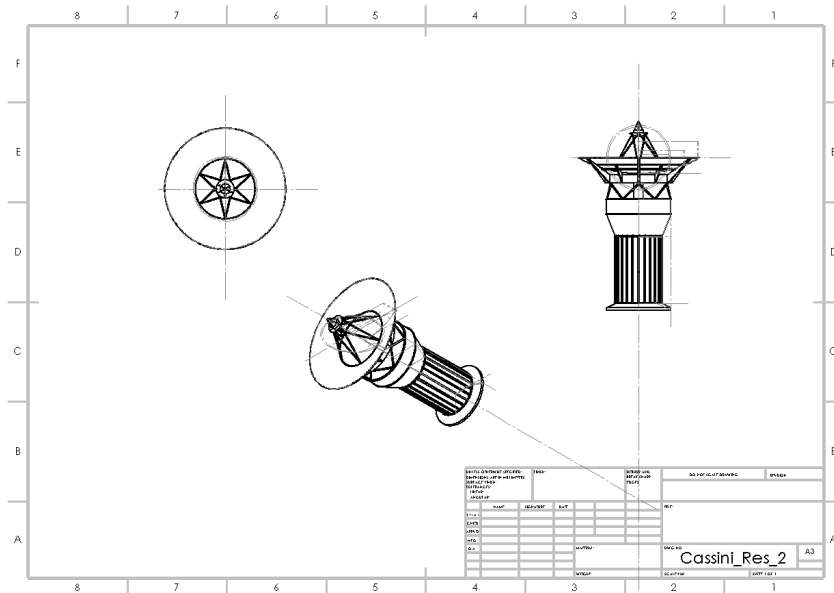


**Figure 1: Cassini Threewiew - created by Pablo Arroyo.**

### 3 Mass Properties - H. Dei

This section addresses the mass and inertial properties of GEORGE, providing intuition for its coordinate axes selection and addressing mass budgets.

#### 3.1 Coordinate Frames

First and foremost, many reference coordinate frames exist for the Center of Mass and Inertial Matrices. In compliance with current literature, we shall use the coordinate frame illustrated below; credit to Mazariko et al. This particular iteration was in the context of the Europa Clipper. Due to the many shared mission requirements between these two projects, it was deemed appropriate for a coordinate system to also be shared. Since this coordinate system has clear flight heritage, and widely-read literature, there is no justifiable reason to change it. This figure provides a diagram with Europa to help visualize positioning at any given instant. These coordinates are always relative to the body, and not relative to its general surroundings. Credit to Kivelson et al. for Figure 2. The origin i.e. reference point would be placed at the geometric center of the body.

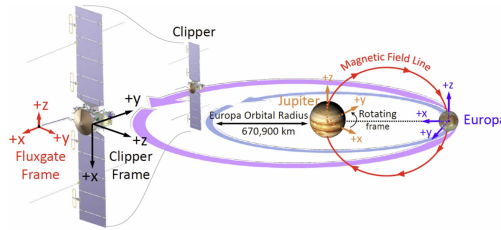


Figure 2: Credit: Europa Clipper Coordinates in Orbit, courtesy of Kivelson et al [3].

#### 3.2 Mass Table & Margins of Safety

The Europa clipper is again taken as a reference point, albeit with several modifications. Margins i.e. Factors of Safety (FOS) shall be computed as:  $FOS = \frac{\text{Measured} - \text{Allowable}}{\text{Allowable}} \times 100\%$ . General considerations are as follows: 20% on physically machined parts, 40% on untested but verified components, 100% on purely theoretical designs and 300% on test stands and testing apparatus. For sub-teams, justifications follow from Wertz, Everett and Michel's Space Mission Engineering, and were updated as necessary.

A MATLAB script has been created to find the inertial matrix, and bookkeep all masses, as well as optimize positions of systems for stability control. This is available via <https://github.com/HillelDei/16.83> under **inertia\_mat\_calc.m**. The MATLAB script uses specific formulae to calculate the inertia matrix and optimize the center of gravity (CG) of a system. The inertia matrix is calculated using the moments of inertia  $I_{xx}, I_{yy}, I_{zz}$  and the products of inertia  $I_{xy}, I_{xz}, I_{yz}$  for each component. These are defined in the appendix, where  $m$  is the mass and  $x, y, z$  are the coordinates of each component. The inertial matrix may be explicitly stated as

**Table 1: Mass Budget.**

Component	Mass (no Margin (kg))	Margin	% Contribution	(X, Y, Z) Coordinates
C&DH	42.4	20%	1.1	3, 0, -0.3
Structures	390	20%	10.0	-0.5, 0, -0.3
ADCS	100.3	20%	2.6	0, 0, -0.2
Comms	45	20%	1.2	-1, -3, +0.2
Power	249.6	20%	6.4	-2.5, 0, +0.3
Propulsion	172.8	20%	4.4	-4.0, 0, 0
Thermal	78	20%	2.0	0, 0, 0
Science	730.9	40%	18.7	+2.5, 3, 0
Propellant	2094.5	10%	53.7	0, 0, 0

follows from summing the individual inertial matrices (in kilogram square meters):

$$\bar{I} = 1.0e+04 \times \begin{bmatrix} 1.0012 & 1.4295 & -0.0268 \\ 1.4295 & 3.1761 & -0.0001 \\ -0.0268 & -0.0001 & 4.1606 \end{bmatrix}$$

For CG optimization, the script minimizes the distance between the CG and a target point. The CG is calculated as the mass-weighted average of the positions and is recorded below in meters:

$$CG = [-0.5939 \quad 1.0825 \quad -0.0154]$$

The optimization uses `fmincon` to adjust the  $x, y, z$  coordinates of each component such that this distance, given by  $\text{distance} = \|CG - \text{Target}\|$ , is minimized. This approach effectively repositions the components to achieve a more desirable CG location, with the inertia matrix recalculated accordingly to reflect the new configuration. The figure below indicates movement from the current CG to the target CG at the reference point.

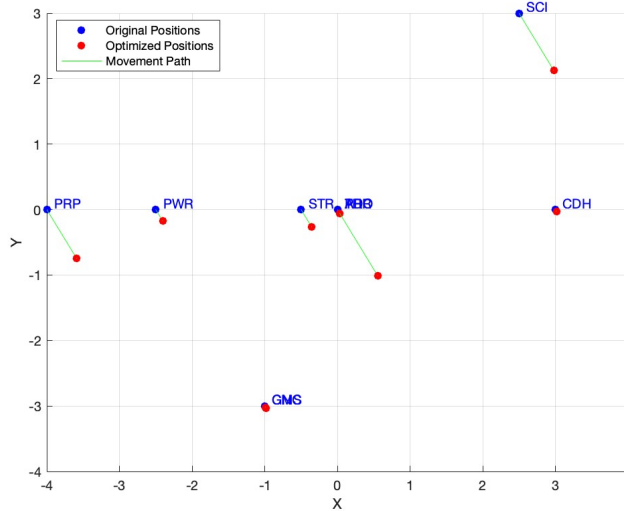


**Figure 3: Subsystem Position and Movement, as point masses - created by Hillel Dei.**

## **4 Materials Selection Trade - Y. Chandar**

There are multiple materials under consideration for the spacecraft bus primary structure. The primary structures main function is to serve as a frame to which science instruments, compute, propulsion, and power systems attach to. The primary structure should minimize mass and cost, maximize stiffness, minimize structural degradation in the transit and destination environments (temperature and radiation), and maximize manufacturability. Flight heritage is preferred due to the limited scope of this mission design. The materials under consideration for the primary structure are 6061 Aluminum T6 alloy, 304L stainless steel, and carbon composite honeycomb panels with aramid core. The cell size for the composite panels is 1/8" and assumed compression loading.

### **4.1 Yield Strength/Density Ratio**

This ratio is in units of Pa\*m\*\*3/kg, resulting in a measurement of the strength to weight ratio.  
6061 Aluminum: 88602 [7]

304L Stainless: 21500 [8]

Carbon Composite: High dependence on custom materials and nonisotropic structures, but in general strength to weight ratio is higher than that of steels and aluminums.

### **4.2 Cost and Density**

6061 Aluminum: 2.50 USD/kg and 2700 kg/m\*\*3 [9]

304L Stainless: 3 USD/kg 8000 kg/m\*\*3 [10]

Carbon Composite: High dependence on custom materials and nonisotropic structures, but in general cost is much higher than of metals and density is much lower.

### **4.3 Environment Characteristics**

6061 Aluminum: Aluminum alloys maintain their mechanical properties and do not degrade significantly in the predicted space environment.

304L Stainless: 300L series stainless steels have favorable mechanical properties in cryogenic environments. The thermal conductivity of stainless steels is lower than aluminum alloys, which can result in heat soak near heat generating components like instruments and computers. The thermal expansion coefficient is  $17.3 \times 10^{-6}/\text{C}$ , lower than 6061. Lower CTE results in lower deformation and stresses due to temperature change, favorable for positioning and tolerancing of components.

Carbon Composite: Composite materials have reduced mechanical capabilities in cold environments. Their brittle nature does not allow for large thermal deformations. Additionally, thermally induced mechanical stresses can occur inside the composite material, leading to cracking and fatigue as the structure repeatedly transitions between sunlit and eclipse regions via rotation and through orbit. Polymer degradation from space radiation is also accelerated, weakening the material over time. This is also an increased risk due to Jupiter's large radiation environment, both in terms of physical size and intensity. Without further testing and bespoke materials, it is hard to characterize the exact properties of the target material.

## **4.4 Manufacturing Considerations**

6061 Aluminum: 6061 Aluminum is available in plate, bar, and round stock, and is machinable. Work hardening is negligible, and complex internal mounting structures can be made with a combination of sheet metal fabrication and machining. Additionally, mechanical properties are similar for both tensile and compressive stresses, allowing for the design and manufacturing of structural members in both tension and compression.

304L Stainless: 304L is available in plate, bar, and round stock, and is machinable with certain constraints. Large parts with many or extensive machining operations are difficult to produce due to work hardening of the steel during machining. This material has excellent weldability, which opens for possible manufacturing methods that rely on welding sheet stock to create the external structure.

Carbon Composite: Carbon Honeycomb panels are difficult to produce and characterize. Additionally, the panels can mainly take stress along the plane of the panel. Structural members must be carefully designed to minimize shear stresses, and stress concentrations (e.g. through holes for fasteners) should be avoided when possible to reduce risk of crushing the honeycomb core. Composite fabrication will involve adhesives and epoxies, which must be minimize offgassing and property changes in the space environment.

## **4.5 Flight Heritage**

6061 Aluminum: Aluminum alloy materials have flown on many previous missions, including Cassini and Europa Clipper.

304L Stainless: 304 and 304L stainless steels are currently used on the Starship launch vehicle.

Carbon Composite: The Juno spacecraft primary structure is made from CFRP panels.

## **4.6 Selection**

GEORGE's primary structure will be constructed from 6061 aluminum or a similar alloy because it has good flight heritage for outer planet missions, has high manufacturability, has the highest strength to density ratio among metal options, and is lowest cost.

# **5 Structural Analysis - H. Dei, P. Arroyo, Y. Chandar**

This section addresses the loading of GEORGE's chassis, and mitigation of possible damage.

## **5.1 Loading Analysis Under Launch Conditions & Dynamic Analysis**

The most significant loading GEORGE experiences will be during launch and internal loading when in orbit. When in orbit, although the force of gravitational attraction is not insignificant, it (approximately) acts evenly around the entirety of GEORGE so its effects are disregarded. As a helpful visualization, the design and loading analysis done follows from works done on Europa Clipper, Cassini, Juno and Juice.

At present, our goal is to launch via a Falcon Heavy due its high weight to orbit and reliability. The image below in Figure 4 depicts the Falcon's Extended Payload Fairing, as specified by the Space Exploration Company (from hereafter referred to as SpaceX) and serves as an upper bound for how much space will be available to design the launch configuration of the GEORGE system. Whilst the ultimate decision came from the Systems subteam, the Falcon Heavy, as will be discussed shortly in this section, meets our dynamic loading requirements and has enough payload volume to accommodate our tentative design with ample space for potential revisions.

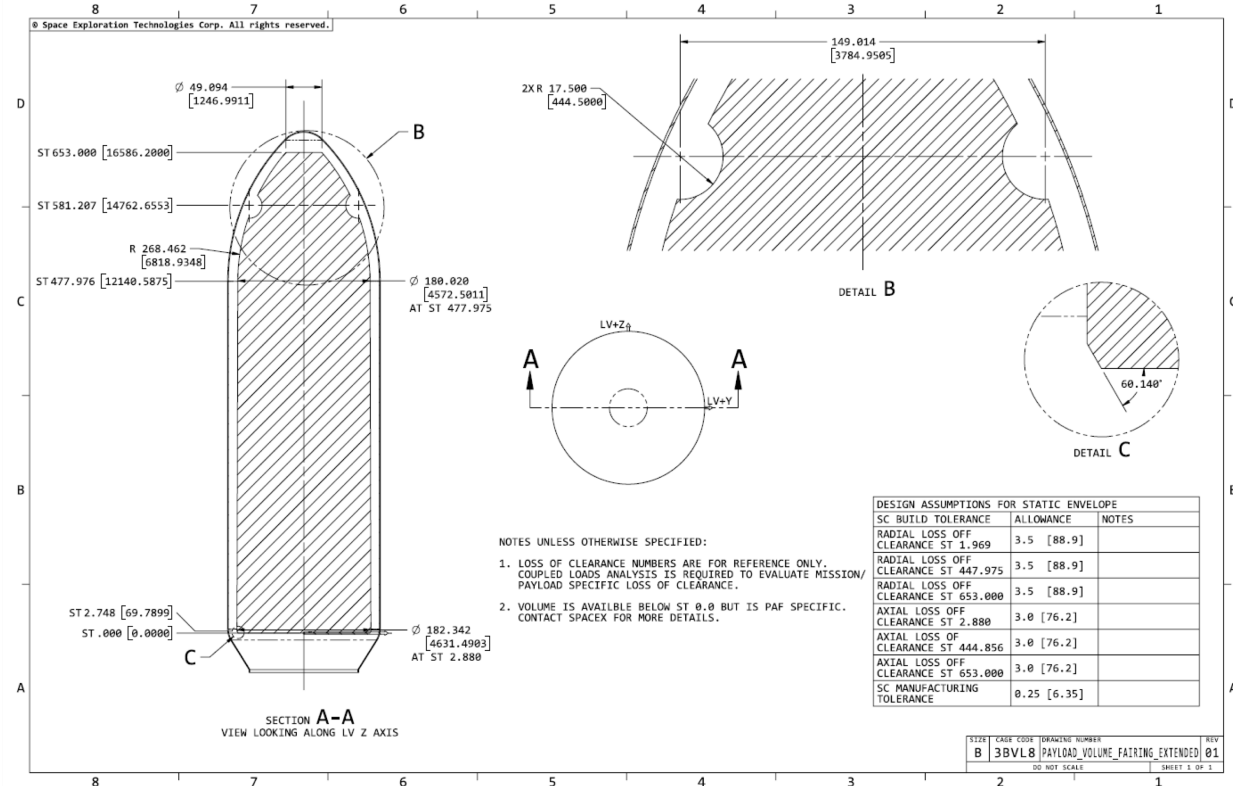


**Figure 4: Falcon Heavy Payload Fairing Dimensions, credit to SpaceX [4].**

To return to our discussion of the dynamic loading of this system, in the specific case of assessing a rocket payload's ability to withstand launch vibrations, the natural frequencies of the payload are compared to the vibrational energy distribution described by the Power Spectral Density (PSD) curve of the rocket. Resonance risk is present if the payload's natural frequencies—ranging from approximately 2.9 Hz to 37.9 Hz—align with peaks in the PSD. For this payload, the RMS response to vibration,  $G_{\text{rms}}$ , is calculated for each mode by integrating the PSD over the frequency range, applying the formula  $G_{\text{rms}} = \sqrt{\int_{f_1}^{f_2} S(f) \cdot H(f) df}$ . The transfer function,  $H(f)$ , for each mode is determined considering the damping ratio ( $\zeta$ ), which is related to the Q factor as  $Q = \frac{1}{2\zeta}$ . The resulting  $G_{\text{rms}}$  values are then used to estimate the induced stresses using  $\sigma = G_{\text{rms}} \cdot m \cdot k$ , where  $m$  is the mass of the payload or component and  $k$  is a stress factor. Fatigue life is subsequently estimated using Miner's rule,  $D = \sum \frac{n_i}{N_i}$ , which sums the damage fractions of stress cycles. Given the data and the modal frequencies falling within the mid-frequency band where the PSD curve rises sharply, there is a potential risk of resonance. However, without precise values for

the damping ratio and the stress factor, a definitive conclusion cannot be reached. Finite element modeling is included below, to model (admittedly with some degree of imprecision) the payload's structural integrity under the expected vibrational loads.

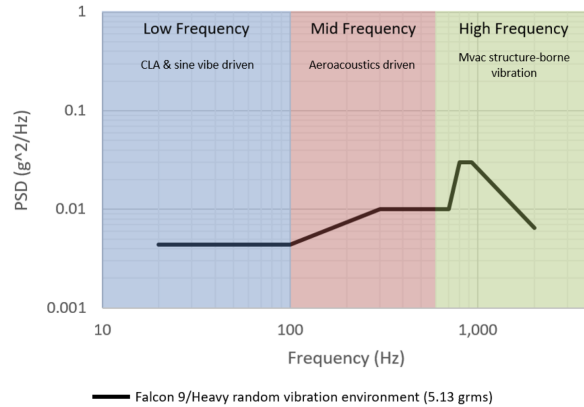


**Figure 5: Falcon Heavy PSD Curve, credit to SpaceX [4].**

The image above in Figure 5 provides a PSD curve, as directly described by SpaceX in their User Manual of the Falcon Heavy under standard launch conditions. With the design drawing heavily from the Cassini Space Probe, the inclusion of a boom is possible. This would suggest the need for acoustic blankets being used, hence the extended Falcon Heavy payload fairing with damping. A preliminary set of simulations was run on the rough SolidWorks model to assess the vibration modes and the response to a given set of frequencies. Ansys will help us evaluate according to the PSD profile mentioned in 5. This was all done assuming 6061 aluminum alloy, which was selected over a composite due to the radiation environment around Europa, as exemplified by the difference in construction materials between the Europa Clipper (mostly aluminum) and the composite-bodied Juno spacecraft. At present, in a hypothetical worst-case scenario where a boom was added and deployed mid-launch, the range of resonance frequencies from 3 to 38 Hertz is cause for concern, and further reinforcement would be necessary. This is because some of the natural frequencies from Figure 12 are within the mid-frequency range, where the PSD curve shows increased energy, suggesting that there is a risk of GEORGE experiencing resonance at these frequencies. A rough model shows tolerance of up to 10g loads; however, the missing structural fins (omitted for simulation time) reduce stiffness and mean there are lower than expected normal vibrational nodes, which should be reduced with ribs added for reinforcement as shown in the higher resolution model. In other words, a boom cannot simply be added and a deployable configuration is necessary for a launch to be more likely to succeed. An example of this is given below in Figure 6 with higher vibrational mode frequencies of 21 to 77 Hertz, although these should ideally be higher. A frequency of at least 100 Hertz should be the design target, as iterations are made, in accordance with historical launches such as those described in the report by Larsen [11].

List Modes

Study name:Frequency 1

Mode No.	Frequency(Rad/sec)	Frequency(Hertz)	Period(Seconds)
1	132.35	21.065	0.047472
2	133.19	21.198	0.047175
3	141.58	22.533	0.04438
4	144.45	22.99	0.043497
5	220.89	35.156	0.028445
6	224.69	35.761	0.027963
7	232.63	37.025	0.027009
8	237.16	37.745	0.026493
9	353.22	56.216	0.017788
10	450.09	71.634	0.01396
11	475.23	75.635	0.013221
12	479.22	76.269	0.013111

**Figure 6: Rough CAD model (without boom) normal mode frequencies created by Pablo Arroyo**

## 5.2 Thermal Stress and Loading Analysis for Heat Redistribution System

The next greatest consideration is the loading on the propulsive module (PM) depending on the alignment of components during launch. For efficiency in packaging, the PM is loaded in-line and orthogonally. The orthogonal loads may cause a swaying effect, analogous to a cantilever beam. If thermal spreaders (i.e. heat lines) for a heat redistribution system are placed along the PM, these extruding (likely aluminum) members may experience strain (and stress) as swaying occurs. They may be designed with specialized bonds and joints to allow for vertical slip to relieve stress. The loading experienced by the PM is illustrated below, with credit to Burdick et al. for the explanation and for the analysis.

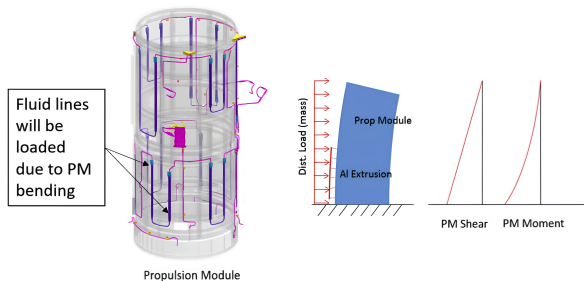


**Figure 7: Illustration of stress on fluid lines during thermal cycling, from of Burdick et al [6].**

In combination with a brace, and a bonding agent, such as Nusil, there should be sufficient resistance to thermal strains due to temperature swings from  $-110^{\circ}\text{C}$  to  $120^{\circ}\text{C}$  and a positive margin for mechanical loading. As acknowledged in Section 5.1, the PM swaying will cause the extrusions to load so they must be capable of withstanding this load. We propose using the hardened stainless steel - treated aluminum joints of the Europa Clipper to mitigate the straining effects. A proposed design and an analysis of the failure limits of these was carried out by Burdick et Al. to the following effect:

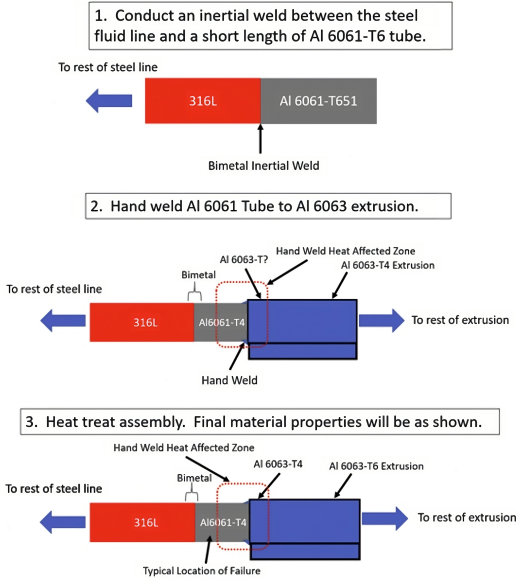


**Figure 8: Inertial welding at material junctions, credit to Burdick et al [6].**

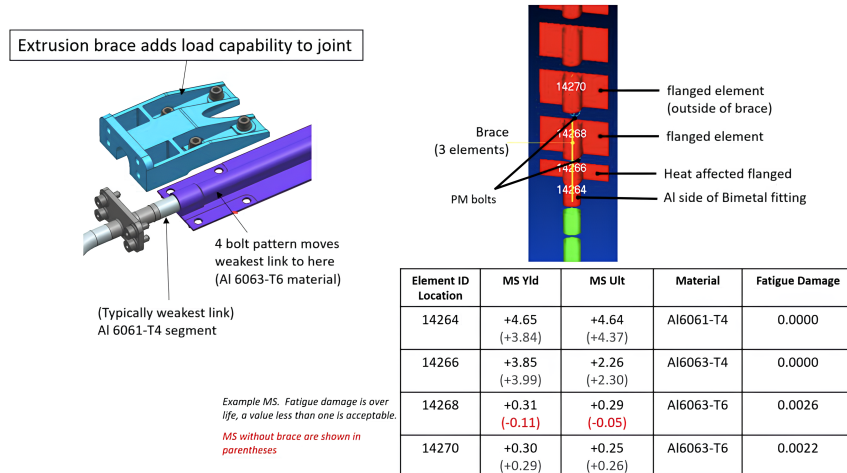


**Figure 9: Joint stresses, credit to Burdick et al [6].**

## 6 Conclusion - H. Dei

The key takeaways from our design choices are that GEORGE will follow from the design choices of successful missions like the Cassini probe. We have provided a preliminary vibrational analysis, demonstrated that it is realistically possible for GEORGE to meet our outlined mass targets, and identified a point-of-departure design. Furthermore, coordinates, inertial matrices, and mass optimization have been provided to inform ultimate design choices. We are confident in the capacity of this mission to deliver, and believe that we have provided a solid structure to be iterated upon.

## References

- [1] Kroon, M., “Solar Arrays for Jovian Missions Juice and Europa Clipper,” *[Online]*. Available: [https://spw.aerospace.org/files/2021/07/2019\\_04\\_02\\_II-b\\_Kroon.pdf](https://spw.aerospace.org/files/2021/07/2019_04_02_II-b_Kroon.pdf). [Accessed Dec. 3, 2023].
- [2] Mazarico, E. et al., “Title of the Article,” *Journal Name*, vol. XX, no. YY, pp. ZZ-AAA, 2023, *[Online]*. Available: <https://link.springer.com/article/10.1007/s11214-023-00972-0>. [Accessed Dec. 3, 2023].
- [3] Kivelson, M. G. et al., “Title of the Article,” *Journal Name*, vol. XX, no. YY, pp. ZZ-AAA, 2023, *[Online]*. Available: <https://link.springer.com/article/10.1007/s11214-023-00989-5>. [Accessed Dec. 3, 2023].
- [4] SpaceX, “Falcon User’s Guide,” SpaceX, 2021, *[Online]*. Available: <https://www.spacex.com/media/falcon-users-guide-2021-09.pdf>. [Accessed Dec. 3, 2023].
- [5] Arya, M., “Title of Thesis,” Ph.D. dissertation, Dept. Eng., California Institute of Technology, Pasadena, CA, 2016, *[Online]*. Available: [https://thesis.library.caltech.edu/9734/1/arya\\_manan\\_2016.pdf](https://thesis.library.caltech.edu/9734/1/arya_manan_2016.pdf). [Accessed Dec. 3, 2023].
- [6] Burdick, J. W. et al., “Title of the Article,” *Journal Name*, vol. XX, no. YY, pp. ZZ-AAA, Year, *[Online]*. Available: <https://ttu-ir.tdl.org/server/api/core/bitstreams/e7644c93-63bc-4c9b-a8bf-d22a461691c8/content>. [Accessed Dec. 3, 2023].
- [7] MatWeb, “Material Data Sheet for 6061-T6 Aluminum,” *[Online]*. Available: <https://asm.matweb.com/search/SpecificMaterial.asp?bassnum=ma6061t6>. [Accessed Dec. 3, 2023].
- [8] MatWeb, “Material Data Sheet,” *[Online]*. Available: [https://www.matweb.com/search/datasheet\\_print.aspx?matguid=e2147b8f727343b0b0d51efe02a6127e](https://www.matweb.com/search/datasheet_print.aspx?matguid=e2147b8f727343b0b0d51efe02a6127e). [Accessed Dec. 3, 2023].
- [9] NavStar Steel, “6061-T6 Aluminum Plate,” *[Online]*. Available: <https://www.navstarsteel.com/6061-t6-aluminium-plate.html>. [Accessed Dec. 3, 2023].
- [10] Global Sources, “304L Stainless Steel Price Per Pound,” *[Online]*. Available: <https://www.globalsources.com/manufacturers/304l-stainless-steel-price-per-pound.html>. [Accessed Dec. 3, 2023].
- [11] Larsen, C., “Title of the NASA Report,” NASA Report Number, NASA, Year, *[Online]*. Available: <https://ntrs.nasa.gov/api/citations/20080018689/downloads/20080018689.pdf>. [Accessed Dec. 3, 2023].

# Appendices

## A L1 Requirements

R ID#	Requirement Title	Requirement
<b>R-1 Mission Design</b>		
R-1.1	Launch Mass	GEORGE's launch mass shall not exceed 4000 kg.
R-1.2	Subsystem Mass Allocations	Subsystems shall not exceed the mass allocations outlined in [TBD document].
R-1.3	Subsystem Power Allocations	Subsystems shall not exceed the power allocations outlined in [TBD document].
R-1.4	Power Generation	GEORGE's overall nominal power generation shall be at minimum 1299.2 W
R-1.26	Launch Envelope	GEORGE's launch dimensions should not exceed the dimensions of a Falcon Heavy fairing
R-1.27	Launch Trajectory	GEORGE shall utilize a trajectory reaching Europa in less than 84 months
R-1.7	Sample Collection	GEORGE shall collect samples from at least 1 plume
R-1.8	Europian Orbit Height	GEORGE shall achieve an apoapsis of 200 +/- 5 km and periapsis of 200 +/- 5 km around Europa.
R-1.29	Full surveillance	GEORGE's shall achieve full surveillance of the surface in 1 month
R-1.31	Stable Orbit	GEORGE shall maintain a stable Europian surveillance orbit
R-1.12	Surface Feature Detection	GEORGE shall be able to detect plume sources on the surface of Europa.
R-1.13	Vapor Collection Capability	GEORGE shall collect enough material to perform mass spectroscopy
R-1.16	Biosignature Detection	GEORGE shall detect concentrations of salts, hydrocarbons, nitrogen, phosphorus, sulfur and oxygen present in collected vapor samples.
R-1.17	Seismic Detection	GEORGE shall test for seismic activity on the Europian surface.

Continued on next page

(Continued)

R-1.30	Earth Contact	GEORGE shall be capable of continued data transmission and contact with Earth through the DSN
R-1.31	Orientation	GEORGE shall have capability of orientation manipulation
R-1.32	Contamination Prevention	GEORGE's mission operations shall adhere to NASA Procedural Requirement (NPR) 8020.12D.

---

**R-2 Environmental Considerations**

---

R-2.1	Temperature Management	GEORGE shall be able to fully operate between 0 and 20 C
R-2.2	Radiation Management	GEORGE shall be able to fully operate after receiving TBD Sv of radiation.
R-2.3	Plume Impact Survival	GEORGE shall survive TBD impacts with Europan plumes.
R-2.4	Plume Detection	GEORGE shall be able to detect Europan plumes in the atmosphere.
R-2.5	Eclipse Survival	GEORGE shall be able to survive at most a 2520 min eclipse.

## B Power System Structure Trade - P. Arroyo, Y. Chandar

The first of our trade studies is for the power system. The power requirements for the spacecraft (instruments, compute, control, communications) must be satisfied by the power system. From a structures perspective, we have two options for satisfying the power budget: RTGs and Solar Arrays. Currently, the power budget with margin is approximately 700W.

### B.1 Solar Arrays

The main structural concerns for solar arrays are their deployable nature, as they have to be folded to fit in the rocket fairing, their fragile construction, as they need to be light and are thus made of thin Silicon or Gallium Arsenide cells. When deployed in the space environment, the arrays will act as large cantilevers and must be supported from the root of the array. Additionally, they will move the mass distribution of the spacecraft further from the rotational axis, increasing the moment of inertia. The mass of the Europa Clipper solar array is 571kg, and will provide an EOL wattage of 728W at 5.8 AU [[Kroon](#)].

### B.2 RTGs

RTGs from a structural perspective are favorable. They are much lighter, and the mass is centralized in the spacecraft bus, resulting in lower moment loadings on extended components during maneuvers. Additionally, they do not have the damage and deploy risks that arrays would have, and can supply heat to temperature-sensitive electronics and batteries on the spacecraft. However, they are more expensive and sourcing these modules is more difficult. The analogues for this mission would be Galileo and Cassini, which used the NASA GPHS-RTG. This RTG has a mass of 55.7 kg, and is 1.14 m long and 0.422 m in diameter. Each RTG will also require .1 inches of lead shielding each. To meet the EOL power budget, 3 RTGs are planned, each with an initial power of 245W [[checksums](#)].

### B.3 Recommendations

Given the flight heritage of both RTGs and solar arrays, they are both viable options for space-craft power. However, JUICE, Europa Clipper, and Juno have all used solar arrays due to the lower cost. RTGs are easier to package, and taking inspiration from Cassini's three RTG modules in the center of the bus would provide favorable MOI benefits and reduce deployable mechanism complexity. Given the benefits of RTGs for packaging, integration, and deployment, GEORGE will use three RTGs.

## C Vibrational Analysis

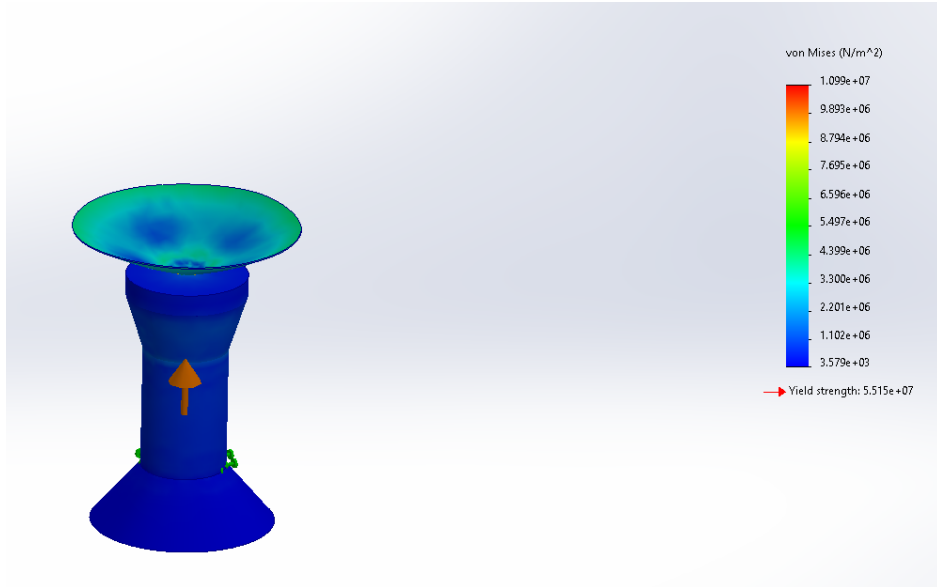


**Figure 10:** Rough CAD model vibration response, without boom deployed; created by Pablo Arroyo

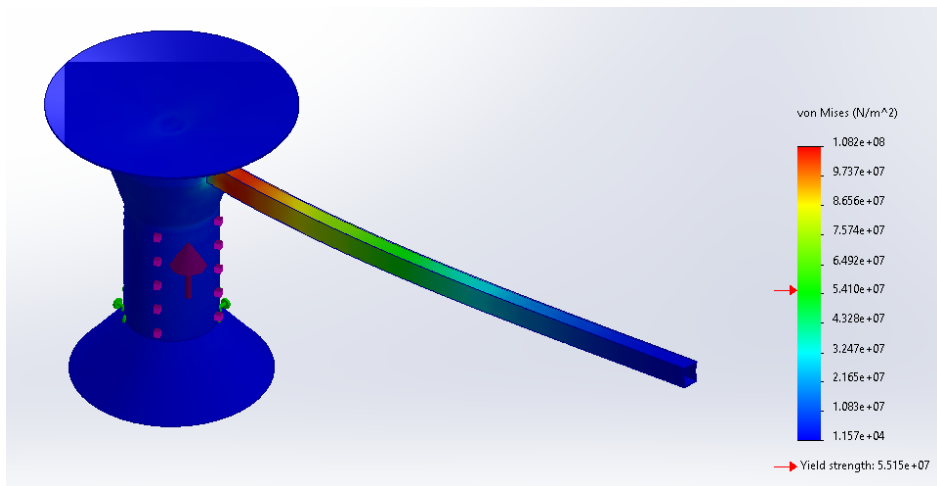


**Figure 11:** Rough CAD model vibration response, with boom deployed; created by Pablo Arroyo

Study name:Frequency 1			
Mode No.	Frequency(Rad/sec)	Frequency(Hertz)	Period(Seconds)
1	18.314	2.9148	0.34308
2	23.657	3.7651	0.2656
3	113.21	18.018	0.055499
4	143.87	22.897	0.043673
5	144.82	23.05	0.043385
6	146.27	23.279	0.042957
7	168.26	26.78	0.037342
8	169.6	26.993	0.037047
9	222.37	35.392	0.028255
10	230.38	36.666	0.027273
11	233.96	37.236	0.026855
12	238.32	37.929	0.026365

**Figure 12:** Rough CAD model vibration response table, with boom deployed; created by Pablo Arroyo

## D Loading Analysis for Deployable Mechanisms

This section may be used as a reference, should any moving (particularly foldable) components be introduced at a later point. Credit to Manan Arya of Stanford University for the figure below, illustrating the loading effects that arise during deployment. To simplify analysis, we shall assume zero (or at most, approximately zero) curvature of whatever body is deploying.

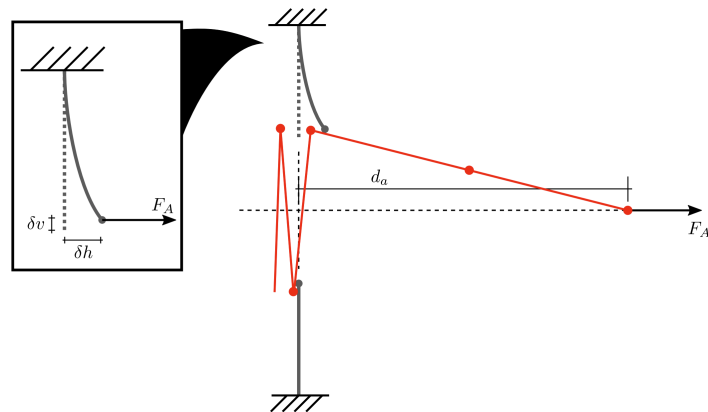


**Figure 13:** Kinematics of solar array deployment, credit to M. Arya [5].

In the above,  $F_A$  represents the deployment force during the actuation i.e. the unfolding process. If the panels are slack, then  $F_A = 0$  but if the panels are taut,  $F_A \geq 0$ . The panel will extend outward until some maximum deflection and/or deformation is reached and then the hinging mechanism can release the next folded element within the array. This effectively constitutes a Free Body Diagram of the Solar Array Arm in Actuation.

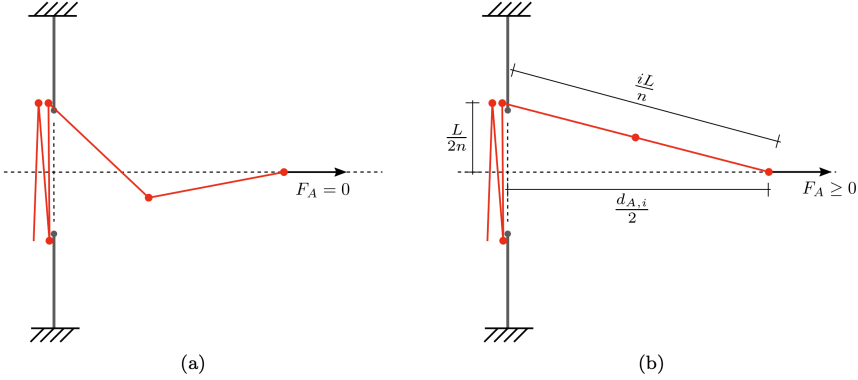


**Figure 14: Force Diagram of solar array deployment, credit to M. Arya [5].**

As Arya describes, simple geometry may be used to evaluate the distance of actuation thanks to Pythagoras's theorem:  $\left(\frac{d_{A,i}}{2}\right)^2 + \left(\frac{L}{2n}\right)^2 = \left(\frac{iL}{n}\right)^2$ . When an arbitrary hinge ( $i + 1$ ) snaps into place, that means the vertical deflection of its tip  $\delta v$  from the tip force  $F_A$  matches the initial overlap between the clip and the hinge. If the flap is treated as an elastic rod with zero extension, simple solid mechanics may be used to derive the horizontal and vertical deflections  $\delta v$  and  $\delta h$  with the maximum length of the deflected flap also being described as  $\delta v = \frac{2}{k}q\cos(\phi_1)$  and then  $\delta h = -\frac{2}{k}[\epsilon(\phi_1; q) - \epsilon(\frac{\pi}{2}; q) - L_f]$  respectively, consistent with Arya's notation.